Published in final edited form as:
J Craniofac Surg. 2012 January ; 23(1): 61–66. doi:10.1097/SCS.0b013e318240c8c4.

Calvarial Cleidocraniodysplasia-like defects with ENU-induced *Nell-1* deficiency

Xinli Zhang, MD, PhD[a,b], **Kang Ting, DMD, DMedSci**[a,b,c,*], **Dharmini Pathmanathan, DDS, PhD**[b], **Theodore Ko, DDS**[b], **Weiwei Chen, BS**[a], **Feng Chen, PhD**[a], **Haofu Lee, PhD**[b], **Aaron W. James, MD**[a], **Ronald K. Siu, MS**[d], **Jia Shen, PhD**[a], **Cymbeline T Culiat, PhD**[e], and **Chia Soo, MD**[c]

[a]Dental and Craniofacial Research Institute, University of California, Los Angeles, California 90095

[b]Section of Orthodontics, School of Dentistry, University of California, Los Angeles 90095

[c]Orthopaedic Surgery, School of Medicine, University of California, California 90095

[d]Department of Bioengineering, School of Engineering, University of California, California 90095

[e]Oak Ridge National Laboratory, Oak Ridge, Tennessee 37830

Abstract

NELL-1, first identified by its overexpression in synostotic cranial sutures, is a novel osteoinductive growth and differentiation factor. In order to further define Nell-1's role in craniofacial patterning, we characterized defects of the *ENU*-induced *Nell-1* deficient (*END*) mice, focusing on both intramembranous and endochondral cranial bones. Results showed that calvarial bones of neonatal *END* mice were reduced in thickness and density, with a phenotype resembling calvarial cleidocraniodysplasia (CCD). In addition, a global reduction in osteoblast markers was observed, including reductions in Runx2, alkaline phosphatase, and osteocalcin. Remarkably, detailed analysis of endochondral bones showed dysplasia as well. The chondrocranium in the END mouse showed enrichment for early, proliferating $Sox9^{+}$ chondrocytes, while in contrast markers of chondrocytes maturation were reduced. These data suggest that Nell-1 is an important growth factor for regulation of osteochondral differentiation, by regulating both Runx2 and Sox9 expression within the calvarium. In summary, Nell-1 is required for normal craniofacial membranous and endochondral skeletal development.

Keywords

Runx2; membranous bone; Sox9; endochondral bone

[*]Correspondence to: Dr. Kang Ting, University of California, Los Angeles10833 Le Conte Avenue, CHS 30-117, Los Angeles, CA 90095, Tel: 310-206-6305; Fax: 310-206-5349; kting@dentistry.ucla.edu.

Disclosure / Duality of Interest

Drs. X.Z. K.T and C.S. are inventors of Nell-1 related patents filed from UCLA. Dr. C.T. C is an inventor of Nell-1 related patents filed from ORNL. Drs. Ting, Soo, and Zhang are co-founders of Bone Biologics Inc., which licensed Nell-1 related patent applications from UCLA. Dr. C.T. C is a founder of NellOne Therapeutics, Inc. which licensed Nell-1 related patent applications from ORNL.

Introduction

Mouse models have been instrumental in investigating the genetic etiology of human diseases. Runx2 (also known as Pebp2αA/Cbfa1/Aml3), a transcription factor of interest in skeletal development, has been studied using mouse models that express Runx2 in various degrees. Based on these studies, Runx2 has been validated as essential to differentiation of both osteoblastic and chondrogenic differentiation [1]. Specifically, Runx2 moderates early events leading to preosteoblast formation and in cartilage, controls chondrocyte hypertrophy [2]. Complete absence of Runx2 in homozygotic null mice ($Runx2^{-/-}$) results in lack of both endochondral and membranous bones [3, 4]. However, Runx2 haploinsufficiency ($Runx2^{+/-}$) results in a phenotype similar to the human condition calvarial cleidocranial dysplasia (CCD). Studies from our laboratory have previously shown that Runx2 transcriptionally regulates *Nell-1* (*Nel*-like molecule, type 1) [5].

NELL-1's importance in bone formation was originally discovered in pathologically fused cranial sutures [6]. A transgenic model of *Nell-1* over-expression exhibits a CS-like phenotype with premature suture closure [7]. Studies of functional molecules upstream of Runx2 such as FGFRs and Twist [8, 9] and other factors [10–13] suggest that signaling pathways in cranial suture regulation converge at the level of Runx2. Recently, we have confirmed Nell-1 as a key functional downstream mediator of Runx2 through an *in vivo* compensatory study by cross-mating *Nell-1* overexpression transgenic mice with *Runx2* haploinsufficient mice and ameliorating the CCD-like defect [14].

In addition, Nell-1 has recently been confirmed to play a significant role in chondrogenic differentiation and endochondral bone formation [15–17]. Currently, Sox9 has been recognized as a critical transcriptional factor controlling the transition of chondrocytes from the proliferative to hypertrophic stages during endochondral bone formation [18]. Our previous studies have revealed that Nell-1 reproducibly inhibits Sox9 expression in cartilaginous tissues [15, 19], however a more detailed analysis has not yet been performed.

Strictly speaking, the Nell-1 deficient mouse identified by Desai *et al.* in their investigations of ENU-induced mutant phenotypes [20] was not a conventional gene knockout model. The authors mapped the ENU mutation to the location of the mouse *Nell-1* gene which results in formation of a stop codon at 502 and consequently a truncated premature Nell-1 product. The resultant mouse has undetectable levels of Nell-1. **E**NU-induced **N**ell-1 **d**eficient (*END*) mice present with neonatal lethality and skeletal defects in the cranial vault, vertebral column, and ribcage [20]. In this study, we chose to limit our analysis to the craniofacial skeleton because of the obvious craniofacial abnormalities in the *Nell-1* overexpressing mice. We focused on the *in vivo* exploration of two critical transcriptional factors, Runx2 and Sox9, in *END* mice in the context of detailed histological examination of calvarial bone and cartilage. Overall, we show that Nell-1 is required for normal craniofacial intramembranous and endochondral skeletal development.

Materials and Methods

Mouse breeding and skeletal staining

Heterozygote carriers (*17R6^{6R}P/+P^{7R}*) of the mutant *Nell-1* deficient mouse gene were generously provided to us from the Mammalian Genetic Research Facility at Oak Ridge National Laboratory (ORNL) (Oak Ridge, TN, USA) and were transferred to with permission of the Chancellor's Animal Research Committee. All animals were housed and handled in accordance with guidelines of the Chancellor's Animal Research Committee of the Office for Protection of Research Subjects at the University of California, Los Angeles. Mice homozygous for the l7R6^{6R} (*Nell-1* KO) mutation were generated by breeding

heterozygote carriers (l7R6^{6R} *P*/+ p^{7R}) which was generated pink-eyed homozygotes (l7R6^{6R} P/ l7R6^{6R} p) and dark-eyed wild type mice (+*P* ^{7R}/+P^{7R}) as previously described [20]. Matings were done overnight and females were examined for the presence of vaginal plugs, E 0.5 dpc (days postcoitum). Fetuses recovered by caesarean section were on days E 14.5, E 16.5, and E 18.5. The *Nell-1* ^{6R} mouse genotypes were identified from DNA extracted from clipped tails of mutant and wildtype mice. The extracted DNA was amplified using micro satellite primers D7Mit 315-L; TGATA ACAAA ACAGT CAGTA TGAAGC, D7Mit 315-RCTGATCCATCTGTATGATGTTACTTG. The skeletal staining with alcian blue and alizarin red on neonatal mice was done following standard protocol [14].

High resolution microcomputed tomography (microCT) imaging and analysis

High resolution microCT (μCT40; Scanco USA, Inc., Southeastern, PA) was used as previously published [15]. A threshold of 120 for 3-D reconstruction was determined empirically by evaluating skeletal image of newborn wild type mouse heads with serial thresholds. The size of the anterior fontanel, the closest distance of the sagittal suture and the average thickness of parietal bone plates at same plane in each group including wild type (n=10) and *Nell-1 KO* (n=10) newborn mice. The cranio-cervical inclination angle formed by long axis of cervical vertebrae (CVT) and the mandibular plane line (MPL), was measured for each group, wild type (n=10) and *Nell-1* KO (n=10) newborn mice. Data are presented as mean ± SD and analyzed with a two tail student *t*-test, with P≤0.05 considered significant.

Real-time quantitative RT-PCR and western blot using RNA and protein from calvarial tissue

Calvarias including frontal, parietal, interparietal, and partial nasal bones without skin and brain tissues were dissected from wild type and ENU Nell-1 KO mice at E14.5, E16.5 and newborn stage. Total RNA with was isolated with TRIzol reagent and purified with DNase (Invitrogen). First strand cDNA was synthesized using reverse transcriptase kit (Invitrogen). RT-PCR reactions were performed using ABI Prism 7300 Real Time (RT-) PCR System. The Taq Man primer- probe sets were purchased (Applied Biosystems, Foster City, CA) for *Nell-1, Runx2, Opn, Bsp2, Sox9, Type II collagen (Col 2a1, Type X collagen, (Col X), Aggrecan*, and *Gapdh* [17, 21]. All data are representatives of experiments performed in triplicate sets and are presented as the fold difference. Student's *t*-test was used to assess significant differences of gene expression with $P \leq 0.05$ considered significant. The western blot of Nell-1 expression was performed only with soluable protein extracted from neonatal calvaria using antibody specific to Nell1-1 as reported previously [19].

Histological analysis

For histology, tissues were fixed in the 10% formalin PBS and embedded in paraffin. Five micron thick sections were baked at 37° C overnight. Hematoxylin and Eosin (H&E) staining was used per standard protocols. Histological specimens were analyzed using the Olympus BX51 microscopes and images acquired using MicroFire digital camera with Picture Frame software (Optronics, Goleta, CA).

Immunohistochemistry

Paraffin embedded sections were deparaffinized and rehydrated. Sections were treated with 3% H2O2 for 20 minutes. Sections were incubated with antibodies against Runx2, osteocalcin (Ocn), Sox 9, and Type X Collagen (Col 10) (Santa Cruz Biotechnology Santa Cruz, CA) and biotinylated anti-rabbit or anti-goat IgG secondary antibody (Vector Laboratories, Burlingame, CA). Positive immunoreactivity was detected using Vectastain ABC and AEC kits (Vector Laboratories) [7] with red positive staining or with Streptavidin

Alexa Fluor 594 conjugate (Molecular Probes). Controls for each antibody consisted of incubation with secondary antibody in the absence of primary antibody.

Results

ENU-induced Nell-1 deficient mice exhibit CCD-like craniofacial skeletal defects

Desai *et al*. previously performed gross examination of the skeletons of the **E**NU-induced ***N****ell-1* **d**eficient (designated as END hereafter) mice at prenatal stage of E18.5 [20]. In the current study, we further examined the craniofacial bone and cartilaginous tissues with high-resolution micro computed tomography (microCT) and skeletal staining of neonatal mice. In general, the *END* newborn mouse was shorter in body length with a down-to-chin tilted head (Fig. 1A, top panel). Knockout of Nell-1 in craniofacial tissues of *END* mice was confirmed by real time PCR and western blot (Fig.1A). *END* mice had decreased craniofacial bone mass including calvarial bone defects, widened sutures and severe underdevelopment of middle ear bones and auricular bony capsule (Fig. 1B). Using microCT, the lateral view of mouse skull confirmed craniofacial bone dysplasia (Fig.1C). The top-down skull view demonstrated markedly enlarged sagittal sutural width and greater anterior and posterior fontanelle patency (Fig.1C). Quantitative microCT data confirmed significant enlargement of the sagittal suture width and reduction of parietal bone thickness in the *END* mice (Fig. 1D). Interestingly, these developmental anomalies seen in *END* mice highly resemble the CCD calvarial defect phenotype described by Otto *et al*. [4] in the *Runx2* heterozygous mutant mice [3]. Next, to evaluate head position of the *END* mouse, we constructed two planes to determine the cervical-cranial angle (Fig. 1E). Results indicated that this angle formed by intersection of the mandibular and cervical vertebrae planes was significantly smaller in the *END* mouse (Fig. 1E). Thus, Nell-1 deficiency resulted in clear hypoplasia of both intramembranous and endochondral bones.

Nell-1 deficiency affects osteogenic differentiation in calvarial bone plate

Next, coronal sections of the neonatal mouse skull were evaluated (Fig. 2A, A',B and B'). Histological analysis revealed significant reduction of parietal bone thickness in *END* mice as compared to wild type littermate. To investigate cellular consequences of Nell-1 deficiency, osteogenic markers in the sagittal suture osteogenic fronts and parietal bones plates were analyzed for ALP activity and Ocn and Runx2 expression by immunohistochemistry. *Nell-1* mutation resulted in a significant decrease in expression levels of ALP, along parietal bone plates and in the sagittal suture (Fig. 2C,C',D and D'). Similarly, the expression levels of Ocn was decreased in the calvarial bones and sutures (Fig. 2E and E'). Notably, nuclear Runx2 staining was significantly decreased, both in number of $Runx2^+$ cells and staining intensity (Fig. 2F and F'). In agreement to histological findings, the mRNA levels of *Ocn* and *Runx2* from calvarial bones of *END* mice were also significantly lower (Fig. 2G and H).

Nell-1 deficiency delays chondrocyte maturation in cartilaginous components of craniofacial tissue

To further understand the progression of chondrocyte development and maturation in *END* mice, we examined the expression levels of Sox 9, early marker of chondrocyte maturation, and Col X, a late marker of hypertrophic chondrocytes [22]. Notably, the cartilaginous components of auricular capsule, mid ear bones and chondrocranium in *END* mice remained delayed in maturation to hypertrophic chondrocytes (Fig. 3A, A', B and B'). The expression of Col X showed a significant decrease (Fig. 3C, C', D and D'). However, immunohistochemistry of the basioccipital bones of the newborn *END* mice revealed an increase in Sox9 expression (Fig. 3E and E'). In addition, Runx2 levels were also affected in cartilaginous tissue in the cranial base with significantly reduced numbers of $Runx2^+$

perichondrial cells in *END* mice (Fig. 3F and F'). These data were confirmed quantitatively by RT-PCR (Fig. 5). These results indicate that the lack of Nell-1 expression leads to disruption of the normal chondrocyte differentiation process in craniofacial tissues. Alterations in chondrogenic related markers in *END* mice provide evidence of Nell-1's role in endochondral ossification.

Significantly reduced Runx2 and elevated Sox9 in craniofacial bones and cartilages during END mice development

Neonatal lethality of the *END* mouse left only embryonic development available for analysis. In this study, we correlated the expression level and tissue distribution patterns of Runx2 and Sox9 in craniofacial bone and cartilages at mid (E14.5) and late (E18.5) embryonic stages (Fig. 4). Results showed that the numbers of positive Runx2 cells at both calvarial bone (Fig. 4A and A') and craniobase cartilage (Fig. 4B,B',C and C') were significantly reduced in *END* tissues at all stages. However, the expression level and the number of Sox9 positive chondrocytes in craniobase cartilage were much higher in *END* as compared to wild type embryos at both E14.5 and E18.5 (Fig. 4D–G').

In order to quantitatively measure changes in gene expression of molecules critical for osteoblastic and chondrogenic differentiation, we performed real time PCR using total RNA from calvaria at multiple stages (Fig. 5). Expectedly, Nell-1 expression levels were barely detectable in the *END* mice at all stages. Similarly, *Opn*, *Bsp2* and *Runx2* also were significantly decreased in *END* samples. Interestingly, the effects on chondrogenic genes were time and stage dependent. *Sox9* and type II collagen (*Col 2*) exhibited a decrease at E14.5 in *END* mice, but significantly increased at the newborn stage. However, later chondrogenic markers including Aggrecan and Type X collagen (*Col 10*) remained undetectable in neonatal *END* mice. This temporal pattern indicated Nell-1's requirement in normal chondrocyte maturation and cartilage development.

Discussion

The craniofacial skeleton is well recognized to ossify through two distinct but related processes: endochondral and intramembranous ossification [23]. The role of Nell-1 in intramembranous bone formation is well established [7, 24]. Loss of function results in delayed membranous bone growth and a CCD-like calvarial phenotype. Here we focused our analysis on the parietal bone, however all intramembranous bones in the END mouse showed gross hypoplasia. In addition, we observe that loss of Nell-1 results in reduced calvarial Runx2 expression and defined this in a temporospatial manner – relative Runx2 and Bsp2 deficiency in the END mouse increases in severity with developmental stage. This *in vivo* observation has clear *in vitro* precedents, as recombinant Nell-1 protein is known to induce both *Runx2* expression and phosphorylation, and conversely Runx2 transcriptionally activates *Nell*-1 [5, 14, 25]. The importance, however, of Nell-1 in endochondral bone formation is a relatively new finding, and one that our study sought to elucidate.

Endochondral ossification is a complex, highly orchestrated process reliant on chondrocyte proliferation, hypertrophy, vascular invasion, chondrocyte apoptosis, and finally ossification (see [26] for a review). Importantly, a defect in any part of this process can have consequences. Conversely Nell-1 may serve to regulate more than one step in this process. Previous related studies have found that exogenous addition of Nell-1 can induce *in vivo* chondrocyte differentiation [15]. In addition, *Nell-1* overexpression mice display distortions of the chondrocranium, including premature hypertrophy and increased chondrocyte apopotosis [16]. Here, through detailed temporospatial analysis of chondrocyte-related gene expression, we observed Nell-1 to have complex ramifications on chondrocyte-related genes

and ultimately dysgenic / dysplastic endochondral bone formation within the craniofacial complex.

Our data suggest that overall loss of Nell-1 has negative effect at some point in the transition from proliferating to hypertrophic chondrocyte. This conclusion is based on detailed histological analysis showing a relative paucity of Col 10^+ hypertrophic chondrocytes in the END mouse. In conjunction, quantitative analysis showed in the END mouse a relative increase in earlier chondrocyte markers *(Sox9, Col2*) at the expense of later markers (*Aggrecan, Col 10*) – data suggestive of a 'road block' in the natural progression of chondrocyte maturation and overall an accumulation of immature chondrocytes (see Fig. 6).

Overall, our histopathologic study of the END craniofacial complex indicates that loss of Nell-1 results in reduced $Runx2^+$ domains and concomitant increase in $Sox9^+$ positive domains (Fig. 6). Recent theories suggest that osteochondroprogenitor cells are $Runx2^+Sox9^+$, and that the balance of these two critical transcription factors influence mesenchymal cell differentiation to osteogenic or chondrogenic cell fates, respectively [27, 28]. Our data in the craniofacial complex suggest that Nell-1 may be one such signaling factor that impacts this cell fate decision.

In summary, loss of Nell-1 in the END mouse results in delay and malformation of craniofacial ossification – negatively effecting both endochondral and intramembranous ossification. Nell-1 is not required for either process, however all bones examined in the END mouse are dysplastic / hypoplastic. Molecular analysis indicates a global reduction in osteogenic gene expression in the END mouse – suggesting that loss of Nell-1 reduces the rate and/or degree of membranous bone deposition. In comparison, the endochondral bone phenotype of END mice is more complex. END mice show a relative enrichment in early, Sox9+, proliferating chondrocytes in combination with a relative paucity of hypertrophic chondrocytes. These data collectively suggest an as yet undefined mechanism through which Nell-1 positively regulates the rate of cartilage maturation. Future studies will elucidate the mechanisms through which Nell-1 regulates cartilage maturation, either via direct effects on chondrocytes or indirect effects through secondary signaling cascades.

Acknowledgments

Sources of Support: This work was supported by the NIH/NIDCR (grants R21 DE0177711 and RO1 DE01607), UC Discovery Grant 07-10677 and the Thomas R. Bales Endowed Chair.

References

1. Kobayashi H, et al. Multilineage differentiation of Cbfa1-deficient calvarial cells in vitro. Biochem Biophys Res Commun. 2000; 273(2):630–636. [PubMed: 10873656]
2. Akiyama H, et al. Positive and negative regulation of chondrogenesis by splice variants of PEBP2alphaA/CBFalpha1 in clonal mouse EC cells, ATDC5. J Cell Physiol. 1999; 181(1):169–178. [PubMed: 10457365]
3. Komori T, et al. Targeted disruption of Cbfa1 results in a complete lack of bone formation owing to maturational arrest of osteoblasts. Cell. 1997; 89(5):755–764. [PubMed: 9182763]
4. Otto F, et al. Cbfa1, a candidate gene for cleidocranial dysplasia syndrome, is essential for osteoblast differentiation and bone development. Cell. 1997; 89(5):765–771. [PubMed: 9182764]
5. Truong T, et al. Craniosynostosis-associated gene nell-1 is regulated by runx2. J Bone Miner Res. 2007; 22(1):7–18. [PubMed: 17042739]
6. Ting K, et al. Human NELL-1 expressed in unilateral coronal synostosis. J Bone Miner Res. 1999; 14(1):80–89. [PubMed: 9893069]
7. Zhang X, et al. Craniosynostosis in transgenic mice overexpressing Nell-1. J Clin Invest. 2002; 110(6):861–870. [PubMed: 12235118]

8. Bialek P, et al. A twist code determines the onset of osteoblast differentiation. Dev Cell. 2004; 6(3): 423–435. [PubMed: 15030764]
9. Zhou YX, et al. A Pro250Arg substitution in mouse Fgfr1 causes increased expression of Cbfa1 and premature fusion of calvarial sutures. Hum Mol Genet. 2000; 9(13):2001–2008. [PubMed: 10942429]
10. Pei Y, et al. Expression of core binding factor alpha1 up-regulated by IGF-I, GM-CSF, and EGF through MAPK pathway in MC3T3-E1 and C2C12 cells. Acta Pharmacol Sin. 2003; 24(10):975–984. [PubMed: 14531938]
11. Lee MH, et al. Transient upregulation of CBFA1 in response to bone morphogenetic protein-2 and transforming growth factor beta1 in C2C12 myogenic cells coincides with suppression of the myogenic phenotype but is not sufficient for osteoblast differentiation. J Cell Biochem. 1999; 73(1):114–125. [PubMed: 10088730]
12. Yamaguchi A, Suda T. Regulation of osteoblast differentiation mediated by bone morphogenetic proteins, hedgehogs, and Cbfa1. Endocr Rev. 2000; 21(4):393–411. [PubMed: 10950158]
13. Javed A, et al. Structural coupling of Smad and Runx2 for execution of the BMP2 osteogenic signal. J Biol Chem. 2008; 283(13):8412–8422. [PubMed: 18204048]
14. Zhang X, et al. Nell-1, a key functional mediator of Runx2, partially rescues calvarial defects in Runx2(+/−) mice. J Bone Miner Res. 2010
15. Cowan CM, et al. Nell-1 induced bone formation within the distracted intermaxillary suture. Bone. 2006; 38(1):48–58. [PubMed: 16243593]
16. Zhang X, et al. Nell-1 induces acrania-like cranioskeletal deformities during mouse embryonic development. Lab Invest. 2006; 86(7):633–644. [PubMed: 16652108]
17. Aghaloo T, et al. Nell-1-induced bone regeneration in calvarial defects. Am J Pathol. 2006; 169(3): 903–915. [PubMed: 16936265]
18. Akiyama H, et al. The transcription factor Sox9 has essential roles in successive steps of the chondrocyte differentiation pathway and is required for expression of Sox5 and Sox6. Genes Dev. 2002; 16(21):2813–2828. [PubMed: 12414734]
19. Aghaloo T, et al. A study of the role of nell-1 gene modified goat bone marrow stromal cells in promoting new bone formation. Mol Ther. 2007; 15(10):1872–1880. [PubMed: 17653100]
20. Desai J, et al. Nell1-deficient mice have reduced expression of extracellular matrix proteins causing cranial and vertebral defects. Hum Mol Genet. 2006; 15(8):1329–1341. [PubMed: 16537572]
21. Chang SC, et al. Rat gene encoding the 78-kDa glucose-regulated protein GRP78: its regulatory sequences and the effect of protein glycosylation on its expression. Proc Natl Acad Sci U S A. 1987; 84(3):680–684. [PubMed: 3468506]
22. Kong RYC, Kwan KM, Lau ET, Thomas JT, Boot-Handford RP, Grant ME, Cheah KSE. Intron-exon structure, alternative use of promoter and expression of the mouse collagen X gene, Col10a-1. Eur J Biochem. 1993; 213:99–111. [PubMed: 8477738]
23. Lenton KA, et al. Cranial suture biology. Curr Top Dev Biol. 2005; 66:287–328. [PubMed: 15797457]
24. Zhang X, et al. Craniofacial Bone Defect in Nell-1 Mutant Mice Associated with Disregulated Runx2 and Osx Expression. J Bone Miner Res. 2008; 23 Suppl:S99.
25. Bokui N, et al. Involvement of MAPK signaling molecules and Runx2 in the NELL1-induced osteoblastic differentiation. FEBS Lett. 2008; 582(2):365–371. [PubMed: 18082140]
26. Wuelling M, Vortkamp A. Transcriptional networks controlling chondrocyte proliferation and differentiation during endochondral ossification. Pediatr Nephrol. 25(4):625–631. [PubMed: 19949815]
27. Zou L, et al. Molecular mechanism of osteochondroprogenitor fate determination during bone formation. Adv Exp Med Biol. 2006; 585:431–441. [PubMed: 17120800]
28. Eames BF, Sharpe PT, Helms JA. Hierarchy revealed in the specification of three skeletal fates by Sox9 and Runx2. Dev Biol. 2004; 274(1):188–200. [PubMed: 15355797]

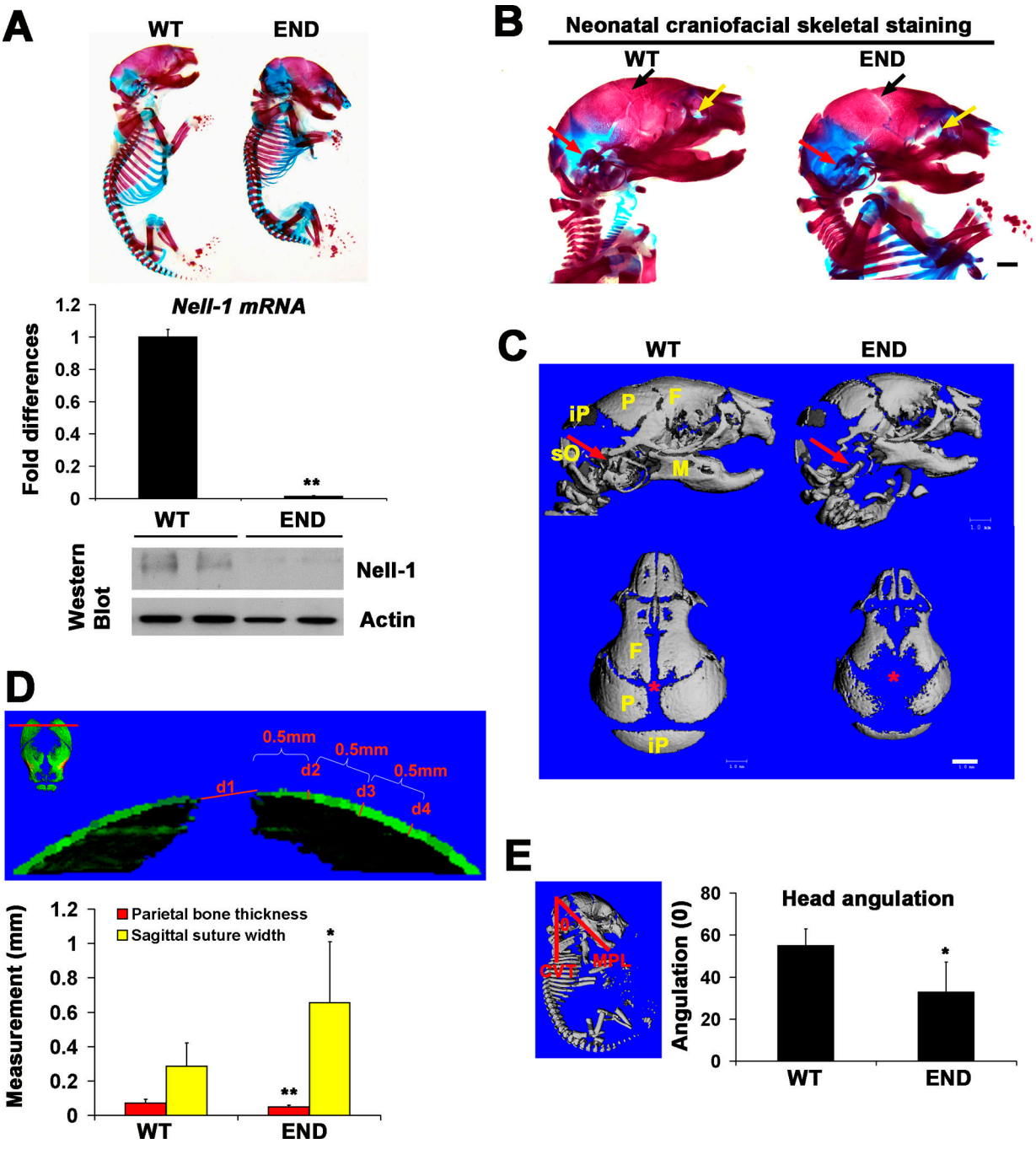

Figure 1.

Craniofacial skeletal features of *END* mice and wildtype mice at newborn stage. (**A**) The skeletal staining of whole mount neonatal *END* mouse and wild type littermate showing overall changes of skeletal system (top panel), and the confirmation of lack of mRNA by real time PCR (middle panel) and Nell-1 protein by Western Blot (bottom panel) from the calvaria of *END* newborns. (**B**) Lateral view of craniofacial skeleton revealed wider coronal sutures (arrows in black), dysplasia of maxillary bones (arrows in yellow) and of auricular bones (arrows in red) in *END* mouse in comparison to wild type littermate. Scale bar: 1mm. (**C**) Lateral and Top view of microCT images of neonatal *END* and wild type skulls demonstrating the difference in cranial bone formation and sutural patency. The red arrows

point to auricular bony capsule and the location of the anterior fontanel of calvaria is marked with red asterisk. *END* images demonstrate widely patent midline sutures and fontanels. Defective mineralization and bone formation is also noted in the *END* mice. F: frontal bone; M: mandible; P: parietal bone; iP: interparietal bone; sO: supraoccipital bone. Scale bar: 1mm. (**D**) The red line drawn through the most prominent points of both parietal bones (top image) indicating a cut-plane with labels d1-d4 (bottom image). The d1 represents sagittal suture width, while d2 through d4 are equal 0.5mm interval measuring points of parietal bone thickness starting from d2. Quantitative analysis of the average width and thickness are depicted graphically with significant differences (**P*<0.05 and ***P*<0.01). (**E**) Depiction of the Head Measurement angulation measurement (left panel). Head angle (°) measured using the angle between two constructed planes, CVT, line representing the long axis of the cervical vertebrae parallel and MPL, mandibular plane line, line representing the mandibular plane. Quantitatative analysis of the head angulation at newborn stage is significantly greater (**P*<0.05) in wild type than that of *END* mice (right graph).

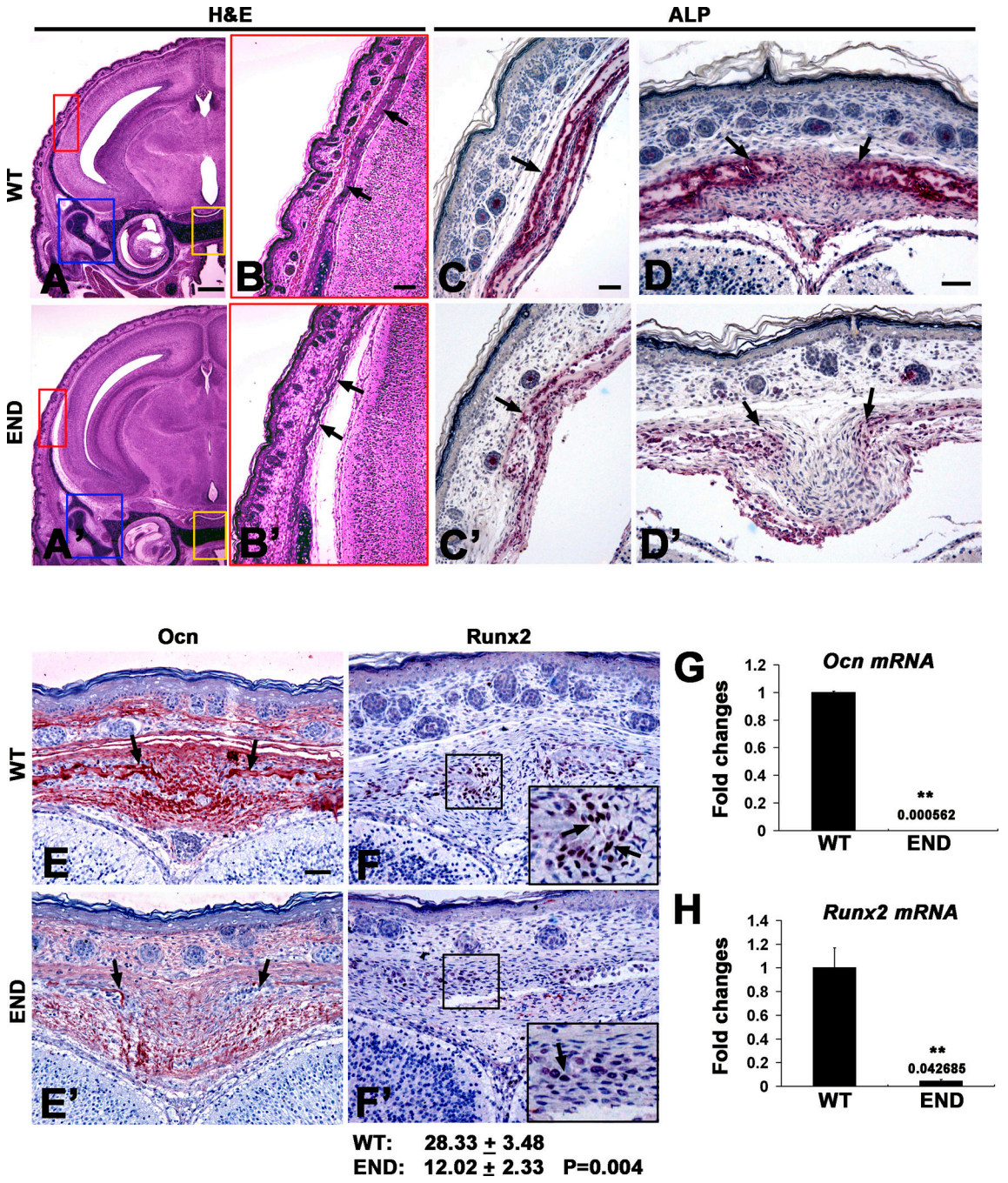

Figure 2.

Histological analysis of defective calvarial bones in *END* mice at newborn stage. (**A** and **B**) H&E coronal sections of wild type and (**A'** and **B'**) *END* mouse heads at newborn stage. The highlighted area in red box magnifies the parietal bone (arrows) showing a much thinner bone plate in *END* (B') than in wild type sample (B). (**C** and **C'**) Wild type and (**D** and **D'**) *END* calvarial bones (single arrow) and the osteogenic front of sutures (arrows) revealed significant difference in ALP activity with much weaker staining intensity in *END* samples. (**E**) Immunohistochemistry of Ocn in the osteogenic front of sutures and calvarial bones (arrows) in wild type sample demonstrated stronger intensity than (**E'**) in *END* calvaria. (**F** and **F'**) Nuclear staining of Runx2 in the osteogenic front of sutures (arrows)

clearly indicated greater numbers of positive cells in wild type than in *END* calvaria. Results were quantitated by average pixel numbers positive staining per 400× field. (**G**) Ocn and (**H**) Runx2 mRNA level by real time PCR with calvarial bone tissue (***P*<0.01). Scale bar: 500um for A and A'; 100um for B and B'; 50um for C,C',D,D',F and F'.

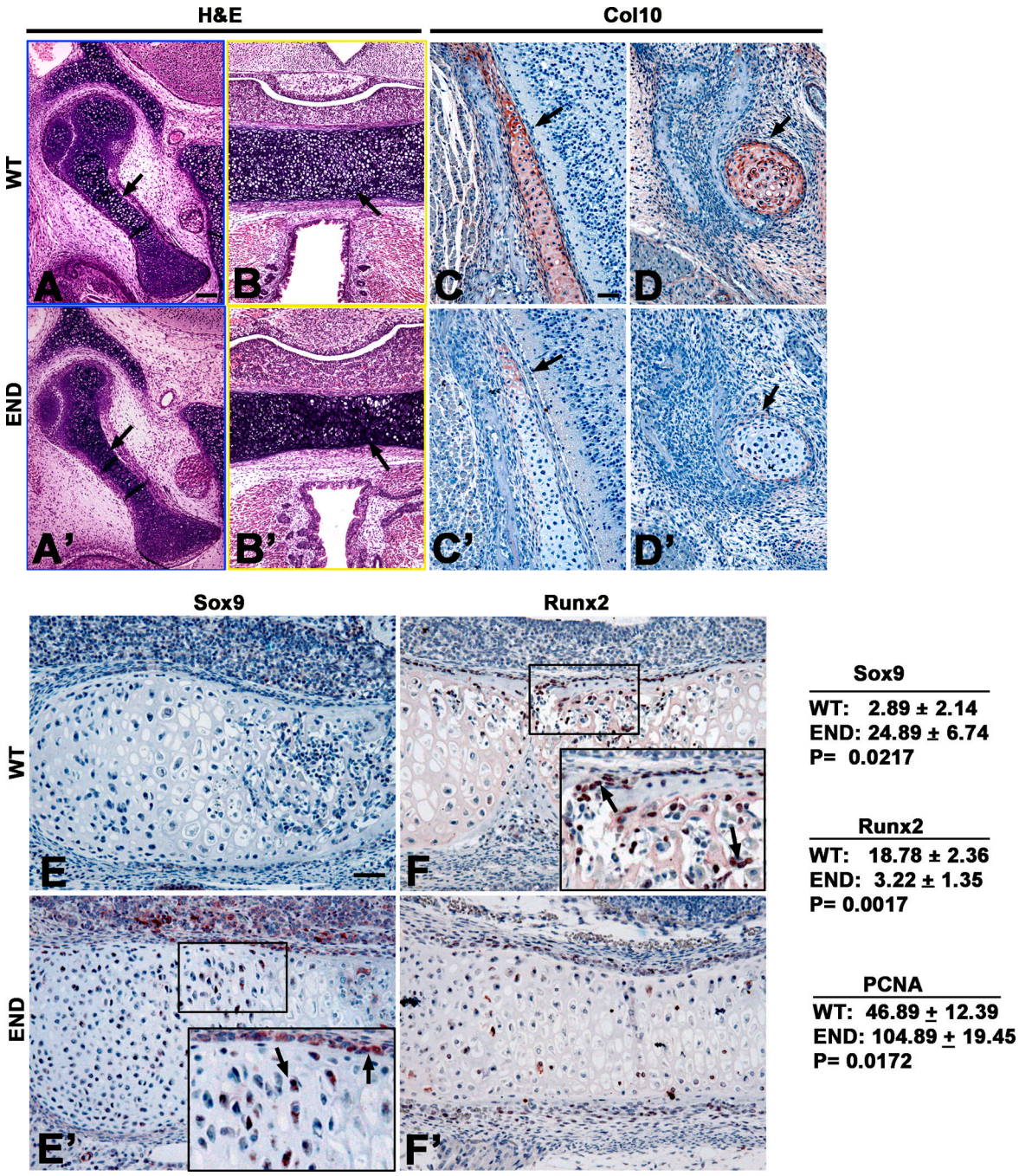

Figure 3.

Chondrogenic characterization of *END* mice at newborn stage. (**A** and **B**) The close up views of middle ear bone (in blue box) and cartilage in craniobase (in yellow box) in Figure 2A showing increased hypertrophic chondrocytes (arrows) in wild type samples than (**A'** and **B'**) in END mouse in Figure 2A'. (**C** and **C'**) The temporal cartilaginous tissue and (**D** and **D'**) Meckel's cartilage were stained much stronger in wild type than in *END* mouse with Col 10 antibody (arrows). (**E** and **E'**) Immunohistochemistry of Sox9 in newborn wildtype cartilage was barely detectable while small number of Sox9 positive chondrocytes (arrows in insert) and perichondral cells was observed with a greater staining intensity in *END* cranial base. (**F** and **F'**) Immunohistochemistry of Runx2 in newborn wildtype cartilage was

significantly stronger and have more positive cells (arrows in insert) while only few positive perichondral cells and chondrocytes were observed in *END* cranial base. Results of Sox9, Runx2, and PCNA immunohistochemistry were quantitated by average pixel numbers positive staining per 400× field. Scale bar: 100um for A, A',B, and B'; 50um for C,C',D,D',E,E',F and F'.

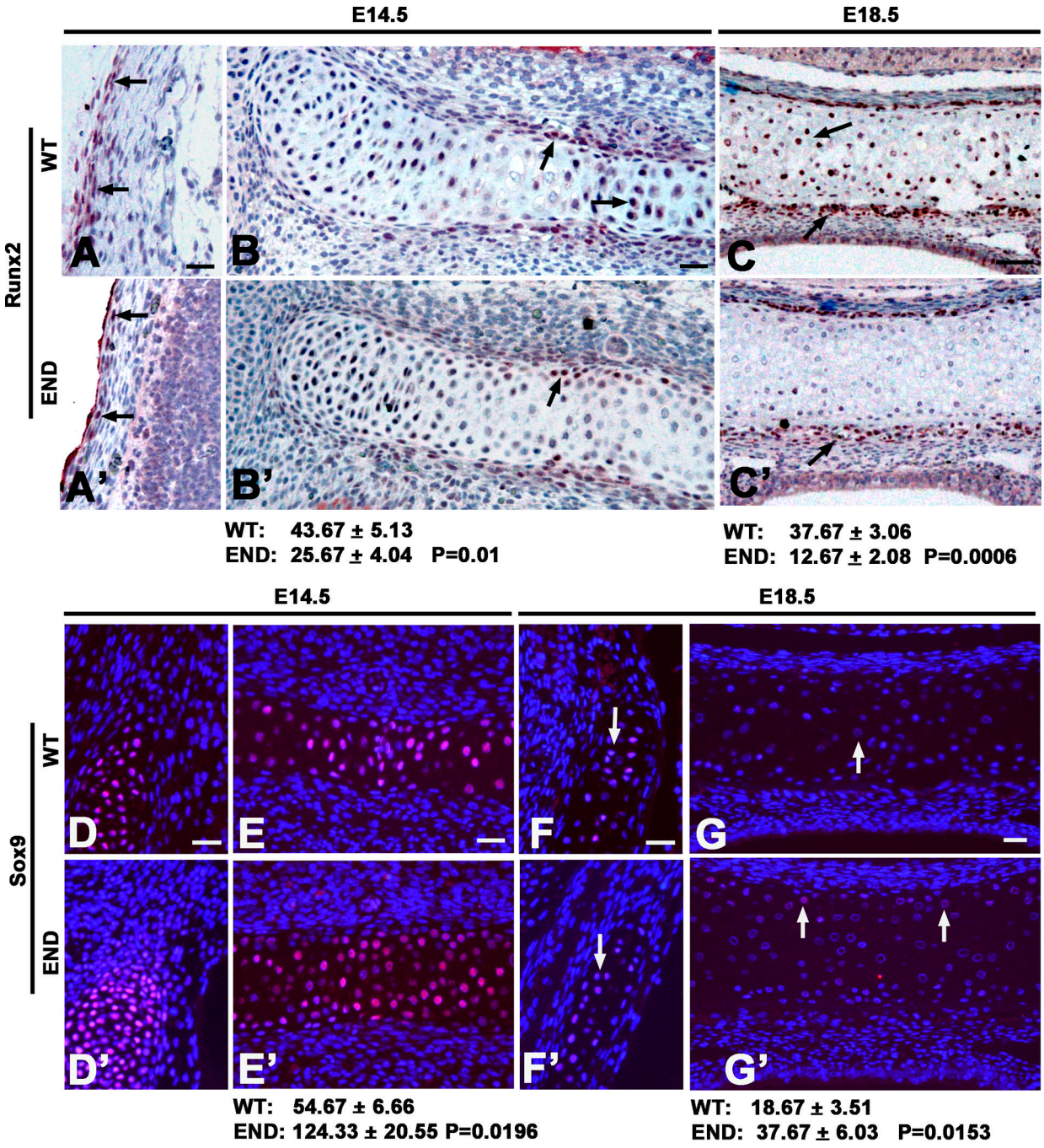

Figure 4.

Runx2 and Sox9 expression in craniofacial bone and cartilage during embryonic development. (**A** and **A'**) Wild type embryos at E14.5 have more Runx2 positive cells along calvarial bone plates than in *END* tissue (arrows). (**B** and **B'**) The cartilages in craniobase at E14.5 and (**C** and **C'**) E18.5 exhibited more Runx2 positive cells in wild type than in END, particularly some prehypertrophic and hypertrophic chondrocytes at E18.5 in wild type mouse (arrows) were strongly stained with Runx2 as compared to END tissue (arrow). In contrast to Runx2, (**D** and **D'**) the temporal cartilaginous tissue and (**E** and **E'**) cranial base at E14.5 revealed large number of Sox9 positive cells in both wild type and END tissues (arrows). However, (**F** and **F'**) the temporal cartilaginous tissue and (**G** and **G'**) cartilage in

cranial base at E18.5 in *END* mouse contained more Sox9 positive chondrocytes than wild type late embryos (arrows), but the staining intensity was significantly less than that at E14.5. Results of Runx2 and Sox9 immunohistochemistry were quantitated by average pixel numbers positive staining per 400× field. Scale bar: 25um for A-**G**'.

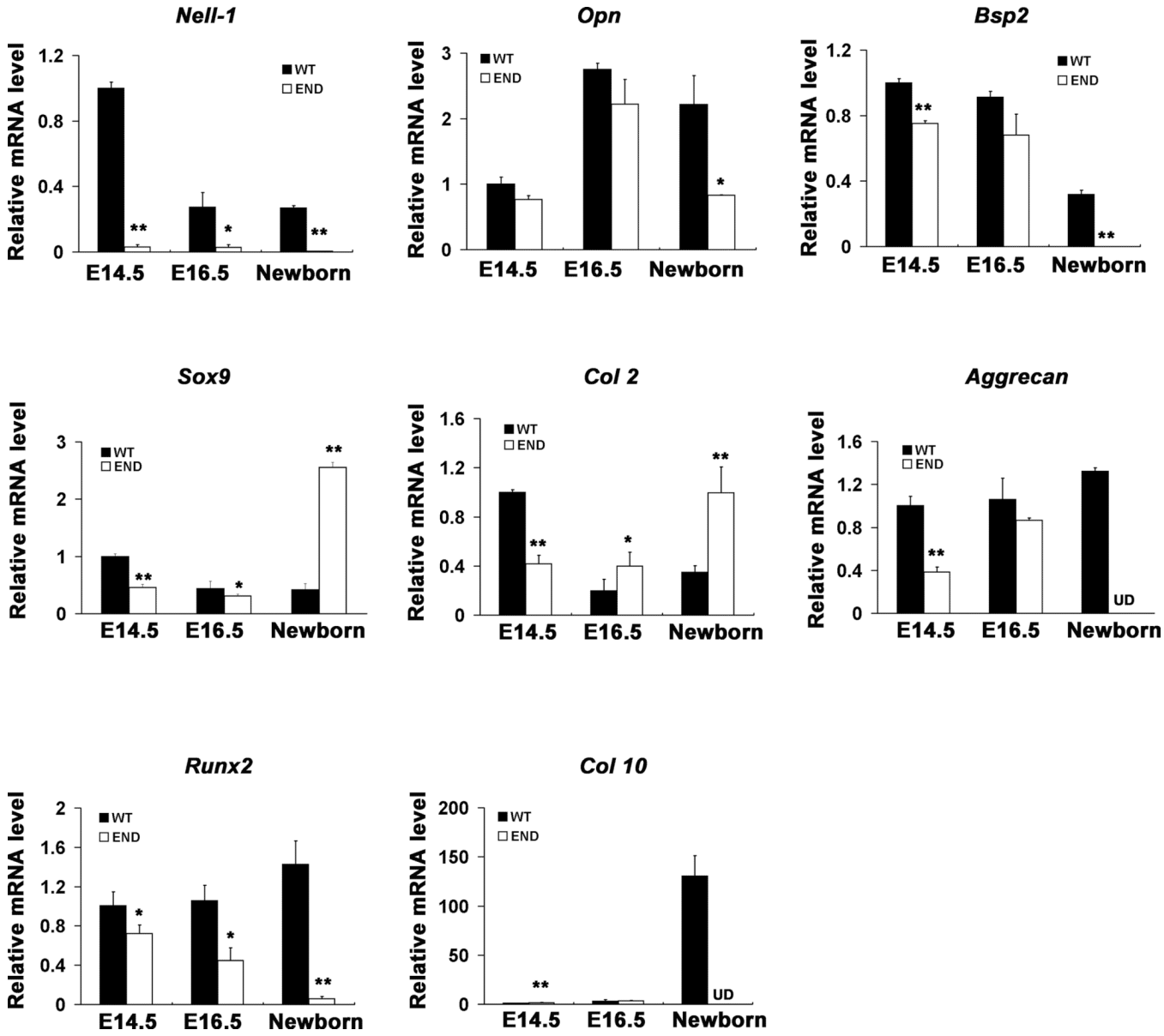

Figure 5.

Gene expression profile in *END* mice compared to wildtype fetuses (E14.5, E16.5) and newborn in calvaria. The level of Nell-1 during the mouse calvarial development was quantitatively detected and further confirmed the knockout nature of Nell-1 in *END* mice or embryos. The osteoblastic differentiation marker genes including Opn, Bsp, Runx2 and the chondrogenic molecules including Col 2, Aggrecan, Col 10 and Sox9 were also detected at embryonic and neonatal stages. The data represents the mean ± SD from tests performed in triplicates. (*P < 0.05; **P < 0.01, UD refers to undetectable levels).

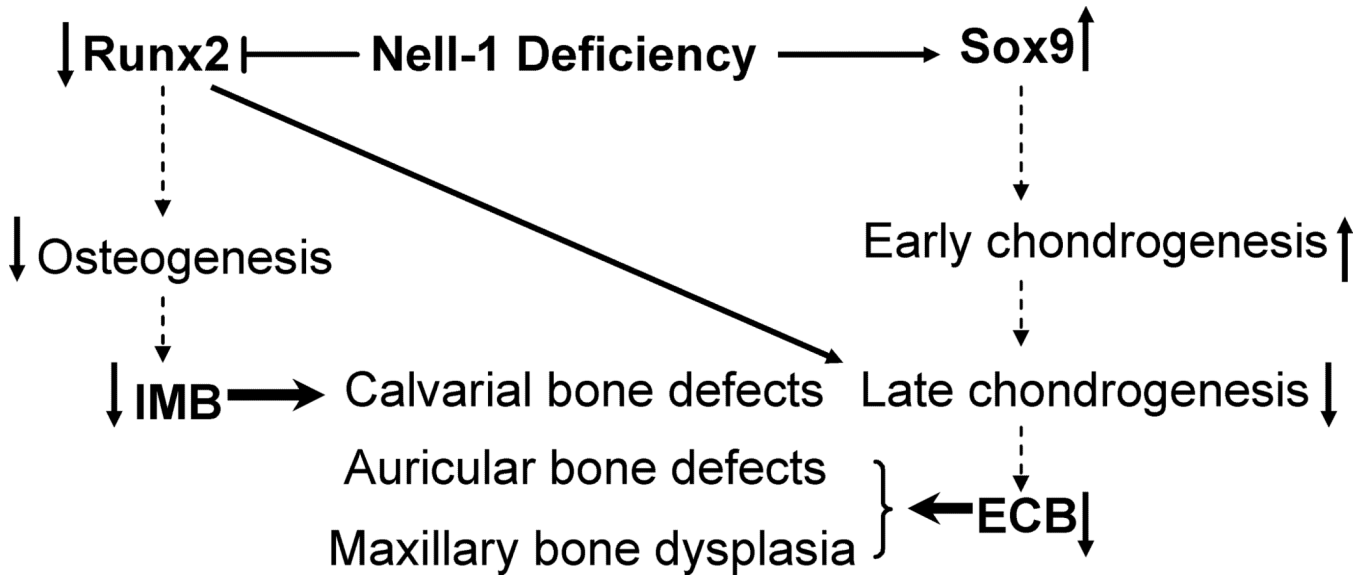

Figure 6.

Schematic diagram of the effects by Nell-1 deficiency in context with alterations of Runx2 and Sox9. The horizontal solid arrows or "T" bar implicate activating or inhibitory effects by Nell-1 deficiency. The vertical solid arrows indicate the up and down gene expression or functional effects. The vertical dotted arrows point to the sequential differentiation. IMB: intramembranous bone formation; ECB: endochondral bone formation.